Modeling the Impact of Polymer Passivation on Graphene FET Stability

Chang Cheng[1]

EEE2209283@xmu.edu.my[1]

School of Artificial Intelligence and Robotics, Xiamen University Malaysia, Selangor, Sepang, Malaysia[1]

Abstract. Graphene Field-Effect Transistors (GFETs) hold immense potential for sensing applications but suffer from severe performance instability in ambient environments due to unintentional p-doping by adsorbed oxygen and moisture. While Polyvinyl Alcohol (PVA) passivation is a promising solution to mitigate this degradation, the quantitative impact of the passivation layer thickness on device characteristics remains under-explored. This paper investigates the stabilizing role of PVA passivation using an analytical modified drift-diffusion model. By incorporating thickness-dependent specific capacitance and the chemical doping effects of hydroxyl groups, the model systematically evaluates how PVA thickness influences the Charge Neutrality Point (CNP) position and carrier transport. Simulation results reveal a critical trade-off: while the PVA layer acts as an n-type dopant to counteract ambient p-doping, excessive thickness functions as a bulk electron reservoir, over-compensating the channel into a unipolar n-type regime. Conversely, optimized thin-film passivation effectively restores the intrinsic ambipolar characteristic and realigns the CNP near zero bias. This study establishes a fast, predictive framework for designing stable, passivated GFETs to counteract environmental degradation without relying on complex numerical simulations or trial-and-error fabrication.

Keywords: GFET, PVA Passivation, Thickness Optimization, Analytical Modeling, CNP Shift

1 Introduction

In recent years, graphene-based devices have been a subject of considerable study in various fields. Among these, graphene field-effect transistors (GFETs) have gathered particular interest from researchers because of their great potential in applications, ranging from chemical detection and biomolecular probing to general-purpose nanoelectronics measurements [1, 2]. Given GFETs' advantages of high carrier mobility, ambipolar transport characteristics, and atomically exposed surface, it is crucial to emphasize the need for achieving stable baseline operation, reducing device-to-device variability, and ensuring long-term electrostatic reliability.

ICMEEA 2026, April 24-26, Singapore, Singapore

DOI 10.4108/eai.24-4-2026.2364892

Ideally, GFET exhibit a symmetric ambipolar transfer characteristic; however, experimental measurements frequently deviate from this theoretical profile due to GFETs' high sensitivity to external perturbations [3]. Due to graphene's extremely low density of states, the Fermi level can rapidly shift with slight adsorption perturbations [4]. Given graphene's low density of states and the inherent energy levels of its ambipolar branches, electrons are readily withdrawn from the channel, leading to a significant hole-dominant p-doping effect with shifted charge charge neutrality point (V_{CNP}), thereby obscuring the electron conduction branch. Consequently, achieving stable baseline operation remains a significant challenge for applications in biosensing and environmental monitoring, as the devices inherently suffer from drift, hysteresis, and heightened device-to-device variability [5].

The instability is rooted in the open and fully exposed graphene channel. Environmental species interact directly with the surface, causing gradual charge transfer and slow trapping–detrapping dynamics that manifest as hysteresis during gate-voltage sweeps [6]. These effects arise independently of fabrication style and remain difficult to suppress without intentional surface engineering. To overcome these issues, polymer-based passivation has been widely reported as a de-facto encapsulation method. Polyvinyl alcohol (PVA), in particular, is noted for hydroxyl (OH^-) functional groups capable of donating electrons to graphene, which can partially restore the charge neutrality point (V_{CNP}) toward zero gate voltage. But experimental data suggested that the film thickness and the film coating formed are greatly different with respect to the film-formation methods (i.e., spin coating and drop casting) [7]. Such a variation in thickness critically affects the strength of charge transfer, the temporal evolution of doping effects, and the stability of the device overall. Notwithstanding this evidence, there is not yet a systematic quantitative analysis of how the thickness of a polymer passivation layer governs its electrostatic and doping behavior.

To bridge this gap, this work adopts a modeling-driven approach to investigate how the thickness of a PVA passivation layer regulates the device physics and stability of graphene field-effect transistors. The remainder of this paper is organized as follows: Section 2 reviews GFET device physics, electrostatic modelling, and passivation mechanisms; Section 3 presents the adopted analytical simulation methodologies; Section 4 discusses modeling results and thickness-dependent device behavior; and Section 5 concludes the study with implications for future GFET design.

2 Theoretical Backgrounds

2.1 GFET Basic Physics and Metrics

GFETs are typically consist of a graphene channel supported by an insulating substrate, with source and drain electrodes defining the transport path. The device operation is governed by the field effect, where a gate voltage V_G modulates the carrier density and type within the channel. This result in a characteristic V-shaped transfer curve ($I_{ds} - V_g$) representing symmetric ambipolar transport. The Dirac point (V_{dirac}), frequently known as the Charge Neutrality Point (CNP), is the lowest possible conductivity point [8], theoretically occurs at $V_{GS} = 0V$.

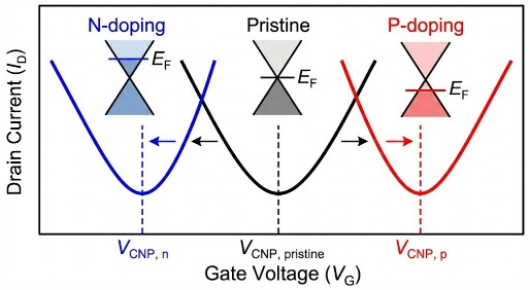

Fig.1. Conical energy band diagram and the associated transport characteristic, Id-Vg curves, of GFETs.

Figure 1 shows the two different-doping GFETs and their transport characteristic curves. If $V_G < V_{Dirac}$, where V_{Dirac} corresponds to the charge neutrality point and signifies the lowest conductivity, the Fermi level lies within the valence band, where holes act as the predominant charge carriers. If $V_G > V_{Dirac}$, the Fermi level shifts into the conduction band and resulting in electrons becoming the majority charge carriers. Typically, positively charged analytes tend to shift V_{Dirac} toward more negative gate voltages. In contrast, the negatively charged target molecules increase the holes density in graphene, leading to a positive shift. Therefore, the left portion of the transfer curve demonstrates a rising density of positive charge carriers (holes), while the right portion indicates an upsurge in negative charge carriers (electrons).

The linear branch of the drain current can be expressed as described by Eq.1 [9]:

$$I_{DS} = \left(\frac{W}{L}\right) \mu C_g V_{DS} (V_G - V_{Dirac}) \tag{1}$$

with the slope g_m (transconductance) being depending on the width (W) and the length (L) of the graphene channel as well as on the mobility of charge carriers (μ) and the gate capacitance (C_g).

2.2 GFET Strucutres and Configuration

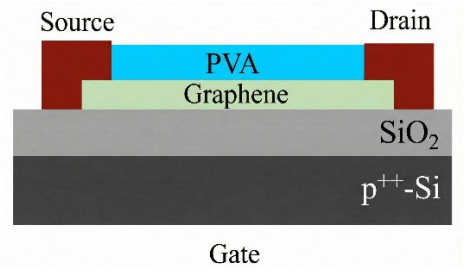

Fig.2 Cross-sectional view of the device structure, showing the PVA layer on top of graphene, supported by SiO_2 and p^{++}-Si substrate

This study utilized the back-gated configuration with a top dielectric passivation layer (Figure 2). Unlike top-gated structures used in logic circuits, the back-gated design leaves the graphene

channel exposed [10]. This establishes a strong foundation for examining the inherent transport characteristics of graphene and the stabilizing influence of solid-state polymer passivation.

2.3 Passivation using Polyvinyl Alchohol(PVA) Physical Barrier and Charge Modulation

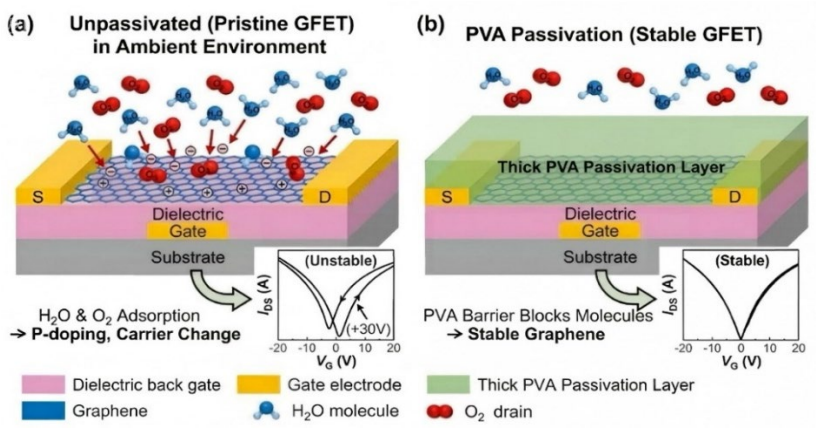

Fig.3 The passivation mechanism shows (a) Unpassivated graphene surface exhibiting p-doping and scattering due to adsorbed atmospheric water and oxygen molecules. (b) GFET stabilized with a PVA passivation layer

The primary function of the passivation layer is to physically isolate the graphene channel from atmospheric adsorbates. The application of a polymer layer (Figure 3) effectively blocks the diffusion of these molecules, thereby suppressing the extrinsic hysteresis caused by the trapping and de-trapping of charges at the interface [11].

The PVA hydroxyl groups act as weak electron donors when in contact with the graphene surface. This electronic interaction compensates for the hole accumulation induced by ambient air, rapidly shifting the positive V_{Dirac} back towards the ideal zero-voltage region [12]. This phenomenon effectively restored the intrinsic bipolar behavior of the p-type doped device whilst maintaining transconductance with negligible degradation.

3 Research Methodology

3.1 Modeling Framework.

To quantify the impact of the passivation layer thickness (d), a modified drift-diffusion model was introduced.

The core of this framework involves modeling the PVA layer as a thickness-dependent equivalent capacitor (C_{PVA}). This component is integrated into the device's overall electrostatic network, where it is coupled with the gate oxide capacitance (C_{ox}) and the quantum capacitance of graphene (C_q) to resolve the potential distribution and carrier transport behavior.

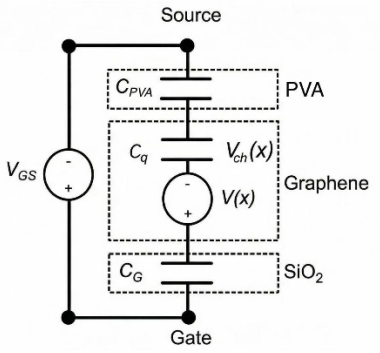

Fig.4 Equivalent circuit diagram of a passivation optimized GFET device.-sectional view of the device

Figure 4 shows the equivalent circuit of the fabricated device. V_x denotes the local potential variation along the channel induced by the bias V_d and C_g is the capacitance of the gate insulator. $V_{ch(x)}$ is the channel potential across the quantum capacitance C_q.

3.2 Modified Drift-Diffusion Model

Based on the drift-diffusion model described in Eq (1), the drain current of the GFET can be expressed as:

$$I_D = \mu W \frac{\int_0^{V_d} |Q_{net}| dV}{L + \mu \left| \int_0^{V_d} \frac{1}{V_{sat}} dV \right|} \tag{2}$$

where μ is the carrier mobility, W and L being the graphene's channel width and channel length, respectively, and Q_{net} denotes the net charge density in the graphene channel [13].
To evaluate the shift of ΔCNP after passivation implementation on the graphene layer, C_{PVA} is incorporated into the charge balance. The shifted net charge density Q_{netSH} is expressed as:

$$Q_{netSH} = \beta s \left\{ \frac{-C_g + \sqrt{C_g^2 + 4\beta \left| C_g \left(V_{gs} - V(x) - V_{PVA} \right) + eN_f + Q_{DNA} \right|}}{2\beta} \right\} \tag{3}$$

Additional parameters, V_{PVA} and Q_{PVA}, have been incorporated into Eq. (3). V_{PVA} is the amount of voltage and Q_{PVA} is the number of charges flow through C_{PVA}. N_f is the fixed charge density, and Q_{PVA} accounts for additional functionalization-induced charges.

$$V_{PVA} = \frac{Q_{netPVA}(x)}{C_{tot}} \tag{4}$$

Where,

$$Q_{netPVA}(x) = -\int C_{tot} dV_{ch} \tag{5}$$

$$\frac{1}{C_{tot}} = \frac{1}{C_q} + \frac{1}{C_{PVA}} \tag{6}$$

$$C_q = \frac{-dQ_{net}(x)}{dV_{ch}} = \frac{2e^2|V_{ch}(x)|}{\pi\left(hV_f\right)^2} \tag{7}$$

$$C_{PVA} = \frac{\epsilon_{PVA}\epsilon_o}{d} \tag{8}$$

ϵ_{PVA} is the constant for the PVA permittivity and d can be regarded as the thickness of the PVA. By substituting Eq. (3)–Eq. (8) into Eq. (2), the drain current of the passivated GFET operating in ambient conditions can be obtained as:

$$I_D = \mu W \frac{\int_0^{V_d} |Q_{netSH}| dV}{L + \mu \left| \int_0^{V_d} \frac{1}{V_{sat}} dV \right|} \tag{9}$$

Based on the parameter set summarized in **Table 1**, numerical simulations are carried out in MATLAB to extract key performance metrics of the GFET, as discussed in the subsequent sections.

Table 1. Parameters utilized for modeling the GFET based on the modified drift-diffusion model

Parameters	**Symbol**	**Values**	**Unit**
Channel Length	L	150	μm
Channel Width	W	50	μm
Oxide Thickness	t_{ox}	120	nm
Passivation Thickness	t_{PVA}, d	0.83~277*	μm
Oxide Permittivity	ϵ_{ox}	3.9	-
PVA Permittivity	ϵ_{PVA}	6-10*	-
Work Function of Metal (Cr/Au)	Φ_M	4.5~4.6	eV
Work Function of Graphene	Φ_G	4.6	eV
Drain Voltage	V_{ds}	2.0	V
Graphene Net doping, N_f (cm^{-2})	N_f	2.3×10^{12}	cm^{-2}
Mobility	μ	6570	cm^{-2}/Vs
Spatial inhomogeneity	Δ	280	meV
Fermi velocity	V_f	10^{8}**	cm/s

Parameter based on [7] and [14]

3.3 Carrier Mobility Extraction

The field-effect mobility was extracted from the linear regime of the transfer characteristics using:

$$\mu = \frac{g_m \cdot L_{ch}}{W_{ch} \cdot C_g \cdot V_{ds}} \tag{10}$$

Where g_m is the transconductance, L_{ch} and W_{ch} denoted the channel length and width. C_g is the gate capacitance, and V_d is the voltage from drain to source. The carrier mobility (μ) is determined from the slope of the $I_{ds} - V_g$ curve within the linear regime.

4 Result and Discussion

The simulation results indicated a distinct divergence in device performance based on the passivation morphology.

4.1 Impact of Ambient Impurities on the Charge Neutrality Point (CNP)

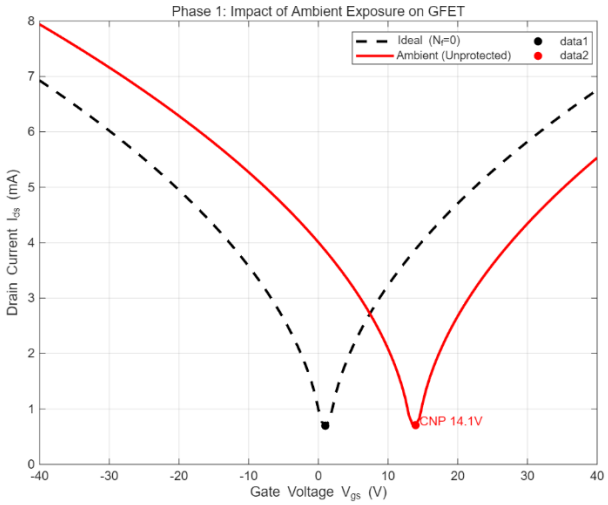

Fig.5 Impact of Ambient Exposure on GFET Devices

Result in Figure 5 illustrates the distinct characteristics of ideal versus ambient-exposed GFETs. The ideal device exhibits minimum conductivity at $V_g = 0V$ with high symmetry, reflecting the intrinsic electron-hole symmetry of pristine graphene. The ambient-exposed device has a CNP shifting to approximately +14V. This physically confirms the role of O_2/H_2O redox couples as electron acceptors. According to the Q_{netSH} term in Eq. (3), the presence of fixed negative interface charges (N_f) induces a substantial built-in electric field in exhibiting positive gate bias to deplete channel holes and accumulate electrons. This rendering the electron branch unobservable within standard scanning ranges.

4.2 Influence of PVA Thickness on Ambipolar Recovery

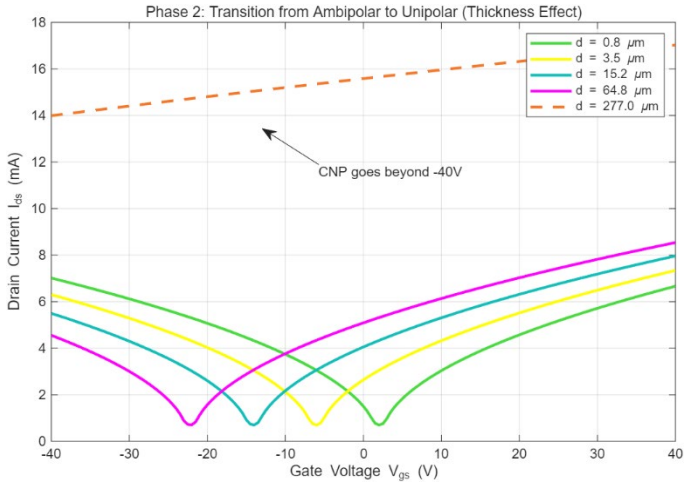

Fig.6 Simulation results of different thickness Effect on the PVA attributes CNP shifts

Figure 6 shows the simulated results with different PVA thickness. In the thin-film regime ($\sim 0.83\ \mu m$), the simulation indicates that PVA-induced n-type doping effectively compensates for residual p-type impurities, restoring V_{CNP} to near $0V$ while maintaining high transconductance via efficient gate coupling. In comparison, increasing thickness to the drop-casting magnitude ($> 100\ \mu m$) degrades performance through two mechanisms. The chemical doping effect introduces excessive hydroxyl groups as electron donors, causing a severe negative drift of the CNP (e.g., beyond -40V) and suppressing hole transport [14]. Second, governed by the series capacitance relation ($C_{PVA} \propto 1/d$), the thick dielectric layer drastically reduces total gate capacitance (C_{tot}). This results in flattened $I_{ds} - V_g$ curves, diminished transconductance (g_m), and a transition to unipolar n-type behavior with a poor on/off ratio.

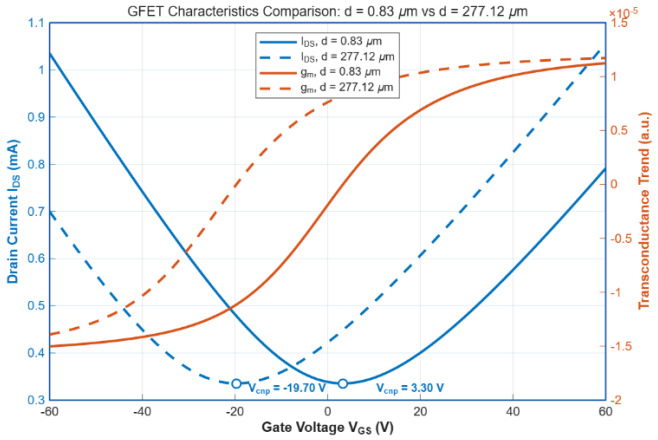

Fig.7 Simulated transconductance (g_m) profile of the thin sc-coated PVA GFET (solid line) and thick dc-coated PVA GFET (dotted line).

The impact of passivation on carrier mobility (μ) was extracted from the transconductance (g_m) of the simulated transfer curves, as shown in Figure 7. The transconductance (g_m) derived from the slope of the $I_{ds} - V_g$ characteristics, calculated as $g_m = \partial I_{ds}/\partial V_g$. For the GFET exposed to ambient, the g_m corresponds to the shifted transfer characteristics with zero point at the CNP (+14V). The strong shift indicates that higher gate drive voltages are needed to achieve the effective modulation regime. The g_m under thick passivation is noticeably reduced across the entire $\pm 40V$ scanning range. This degradation result from the increased thickness, which makes the channel insensitive to gate voltage modulation.

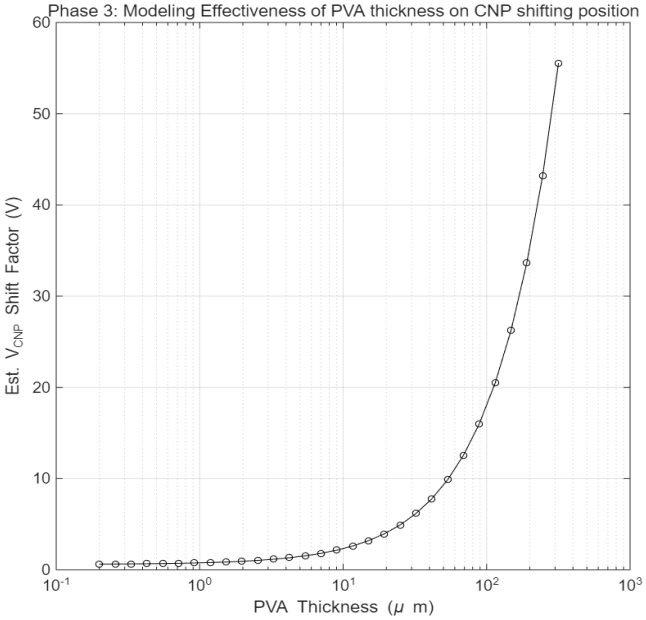

Fig.8 Effectiveness of PVA thickness on CNP shifting position

The logarithmic plot in Figure 8 reveals the non-linear correlation between PVA thickness and V_{CNP}. By comparing the thin (thickness <100μm) configurations, the thin spin-coated layer retains a more balanced electron and hole mobility, maintaining the device's ambipolar nature. On the other hand, due to the excessive electron accumulation in the thicker polymer bulk, the transport asymmetry of the thick layer causes a drastic decrease in hole mobility, this causes the V_{CNP} shifts to exceed the DC sweeping range of $\pm 40V$.

4.3 Hysteresis in Thin-Film PVA Passivated GFET

This section presents the hysteresis loops in both forward and backward sweeping. The CNP of the loop undergoes to a slight shift to +8V. The result reproduce the experimentally observed hysteresis due to charge trapping, which is attributed to the interaction of charge trapping dynamics. Carriers are gradually trapped by interface traps in the forward sweep, and becacuse of the large time constant (τ), the screening electric field formed by these trapped charges remains during the reverse sweep, inducing a voltage shift in the backward curve.

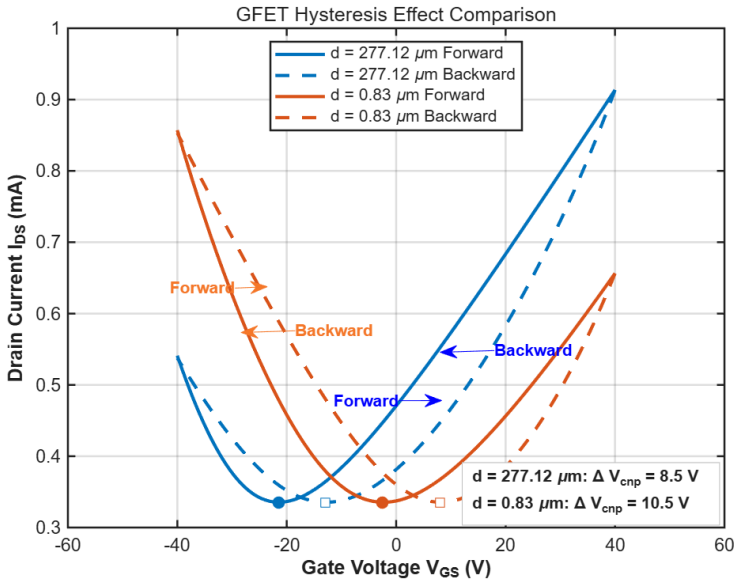

Fig. 9 Simulated transfer characteristics of the sc-coated (thin) and dc-coated (thick) PVA GFET after 24 hours of ambient exposure

Figure 9 displays the simulated transfer characteristics for both thin spin-coated (sc-coated) and thick drop-casted (dc-coated) PVA GFETs following 24 hours of exposure to ambient conditions. The passivation mechanism is validated by the reducing the trap density (N_{trap}), representing the PVA layer's ability to cover surface defects and block water molecules, the primary source of slow traps [15]. Consequently, the hysteresis window narrows significantly, consistent with experimental stability improvements.

The simulation also reports that the hysteresis reintegration, following prolonged indoor environmental exposure, is the product of moisture re-absorption, which is reflected in the higher trap density and permittivity within the PVA film.

5 Conclusion

This work has modeled and analyzed the stability mechanisms of the back-gated GFET under different Polyvinyl Alcohol (PVA) passivation conditions using the MATLAB for numerical solutions. With a modified drift-diffusion model, the study further investigated the correlation between the passivation layer thickness and the hysteresis and carrier transport characteristics of the setting device. Based on the passivation morphology, the output of the simulation showed a clear deviation on device performance using different model parameters. For the thick passivation scenario, which corresponds to the drop-casting method (100-300μm), the device was observed to lose its intrinsic ambipolar behavior over the simulation period. This phenomenon is attributed to the bulk reservoir effect, where the abundant hydroxyl (-OH) groups within the thick polymer matrix act as continuous electron donors. The resulting

excessive n-type doping shifts the Charge Neutrality Point (CNP) significantly and suppresses hole transport, effectively converting the GFET into a unipolar n-type device.

On the contrary, the thin passivation (~0.8 μm) was reported to maintain the ambipolar characteristics, as the decrease in volume restricted the total number of potential electron donors that could be utilized, preventing the severe over-doping seen in thicker films. These findings underscore the sensitivity of long-channel GFETs to passivation volume in drift-diffusion modeling contexts. Rather than prescribing a universal thickness, the study highlights the necessity of optimizing the passivation strategy to balance the trade-off between effective environmental isolation and the preservation of intrinsic symmetric transport properties.

Acknowledgment

The authors are grateful to Xiamen University Malaysia for providing the necessary software licenses and computational resources used in this study. Special thanks go to Dr. Nadia for providing the experimental baseline data and the foundational drift-diffusion framework that made this simulation study possible.

References

[1] J. Mouro, T. Domingues, T. Pereira, R. Campos, J. Borme, and P. Alpuim, "Analytical modeling and experimental characterization of drift in electrolyte-gated graphene field-effect transistors," npj 2D Materials and Applications, vol. 9, no. 1, Apr. 2025, doi: 10.1038/s41699-025-00547-3.

[2] V. D. Camiola, G. Nastasi, and V. Romano, "A drift-diffusion model for charge transport in GFETs with a proper modeling of the electrostatic potential," Journal of Mathematics in Industry, vol. 15, no. 1, Mar. 2025, doi: 10.1186/s13362-025-00171-2.

[3] S. Szunerits, T. Rodrigues, R. Bagale, H. Happy, R. Boukherroub, and W. Knoll, "Graphene-based field-effect transistors for biosensing: where is the field heading to?," Analytical and Bioanalytical Chemistry, vol. 416, no. 9. Springer Science+Business Media, p. 2137, Jun. 03, 2023. doi: 10.1007/s00216-023-04760-1.

[4] S. Wang, X. Qi, D. Hao, R. Moro, Y. Ma, and L. Ma, "Review—Recent Advances in Graphene-Based Field-Effect-Transistor Biosensors: A Review on Biosensor Designing Strategy," Journal of The Electrochemical Society, vol. 169, no. 2. Institute of Physics, p. 27509, Jan. 26, 2022. doi: 10.1149/1945-7111/ac4f24.

[5] Béraud, M. Sauvage, C. M. Bazán, M. Tie, A. Bencherif, and D. Bouilly, "Graphene field-effect transistors as bioanalytical sensors: design, operation and performance," The Analyst, vol. 146, no. 2. Royal Society of Chemistry, p. 403, Nov. 19, 2020. doi: 10.1039/d0an01661f.

[6] D. V. Shtansky, A. T. Matveev, E. S. Permyakova, D. V. Leybo, A. S. Konopatsky, and П. Б. Сорокин, "Recent Progress in Fabrication and Application of BN Nanostructures and BN-Based Nanohybrids," Nanomaterials, vol. 12, no. 16. Multidisciplinary Digital Publishing Institute, p. 2810, Aug. 16, 2022. doi: 10.3390/nano12162810.

[7] N. Norhakim, H. F. Hawari, and Z. A. Burhanudin, "Effect of Thickness of the Poly(vinyl alcohol) Passivation Layer on Ambipolar Characteristics of Graphene Field-effect Transistor," p. 55, Dec. 2022, doi: 10.1109/icftsc57269.2022.10039724.

[8] F. Schwierz, “Graphene transistors,” Nature Nanotechnology, vol. 5, no. 7, p. 487, May 2010, doi: 10.1038/nnano.2010.89.
[9] H. He et al., “Uniform doping of graphene close to the Dirac point by polymer-assisted assembly of molecular dopants,” Nature Communications, vol. 9, no. 1, Sep. 2018, doi: 10.1038/s41467-018-06352-5.
[10] M. Akbari, M. J. Shahbazzadeh, L. L. Spada, and A. Khajehzadeh, “The Graphene Field Effect Transistor Modeling Based on an Optimized Ambipolar Virtual Source Model for DNA Detection,” Applied Sciences, vol. 11, no. 17, p. 8114, Aug. 2021, doi: 10.3390/app11178114.
[11] L. Yang et al., “Revealing the interrelation between hydrogen bonds and interfaces in graphene/PVA composites towards highly electrical conductivity,” Chemical Engineering Journal, vol. 383, p. 123126, Oct. 2019, doi: 10.1016/j.cej.2019.123126.
[12] N. Lu, L. Wang, L. Li, and M. Liu, “A review for compact model of graphene field-effect transistors,” Chinese Physics B, vol. 26, no. 3. IOP Publishing, p. 36804, Mar. 01, 2017. doi: 10.1088/1674-1056/26/3/036804.
[13] Simionescu et al., “Field-Effect Transistors Based on Single-Layer Graphene and Graphene-Derived Materials,” Micromachines, vol. 14, no. 6, p. 1096, May 2023, doi: 10.3390/mi14061096.
[14] P. L. Levesque et al., “Probing Charge Transfer at Surfaces Using Graphene Transistors,” Nano Letters, vol. 11, no. 1, pp. 132–137, Dec. 2010, doi: 10.1021/nl103015w.
[15] N. Norhakim and Z. A. Burhanudin, “Correlation of charge neutrality point and ions capture in DNA-graphene field-effect transistor using drift-diffusion model,” p. 1, Jul. 2019, doi: 10.1109/sensorsnano44414.2019.8940096.